Draft version February 2, 2008
Preprint typeset using LaTeX style emulateapj v. 11/12/01

THE EXPANSION OF G11.2−0.3, A RADIO COMPOSITE SUPERNOVA REMNANT

Cindy Tam and Mallory S. E. Roberts [1]
Department of Physics, Ernest Rutherford Physics Building, McGill University, 3600 University Street, Montreal, Quebec, H3A 2T8, Canada; tamc@physics.mcgill.ca, roberts@physics.mcgill.ca
Draft version February 2, 2008

ABSTRACT

We compare recent observations of the supernova remnant G11.2−0.3 taken with the VLA during 2001−02 with images from VLA archives (1984−85) to detect and measure the amount of expansion that has occurred during 17 years. The bright, circular outer shell shows a mean expansion of $(0.71 \pm 0.15)\%$ and $(0.50 \pm 0.17)\%$, from 20- and 6-cm data, respectively, which corresponds to a rate of $0\farcs057 \pm 0\farcs012$/yr at 20 cm and $0\farcs040 \pm 0\farcs013$/yr at 6 cm. From this result, we estimate the age of the remnant to be roughly between 960 and 3400 years old, according to theoretical models of supernova evolution. This is highly inconsistent with the 24000 yr characteristic age of PSR J1811−1925, located at the remnant's center, but, rather, is consistent with the time since the historical supernova observed in 386 AD. We also predict that G11.2−0.3 is currently in a pre-Sedov evolutionary state, and set constraints on the distance to the remnant based on Chandra X-ray spectral results.

Subject headings: pulsars: individual (PSR J1811−1925) — supernovae: individual (G11.2−0.3) — supernova remnants

1. INTRODUCTION

The process of supernova remnant expansion evolution has long been the subject of thorough investigation, and as a result we can be confident of a few well established facts. In the initial free expansion stage, a tremendous amount of energy in the form of material ejecta is thrown outwards in a (assumed) spherically symmetric explosion, driving a shock wave into the ambient medium. Later, when the mass of the swept-up material considerably exceeds the ejected material mass, the supernova remnant enters the Sedov stage (Sedov 1993), as a reverse shock reaches the center of the remnant and the forward shock undergoes significant deceleration. This simple picture is complicated by the presence of a pulsar wind nebula expanding within, but separate from, the SNR bubble (Chevalier 1984; Reynolds & Chevalier 1984). It eventually encounters the reverse shock, which induces complicated radial reverberations, before relaxing into Sedov phase expansion (van der Swaluw et al. 2001; Blondin, Chevalier, & Frierson 2001). Each stage of evolution can be described by the expansion parameter m, defined by $R \propto t^m$, where R is the linear radius and t is the remnant age.

In G11.2−0.3, we find a textbook example of a composite supernova remnant (SNR) comprising an extremely circular radio and X-ray shell, a pulsar wind nebula (PWN) contained within the SNR (Vasisht et al. 1996; Kothes & Reich 2001), and an X-ray pulsar PSR J1811−1925 (Torii et al. 1997) located at the center. Its high surface brightness and the extremely centralized position of the pulsar within the remnant imply that it is much younger than the pulsar's characteristic age, $\tau = 24000$ yr (Torii et al. 1999; Kaspi et al. 2001), and support the possible association with the historical supernova (SN) event of 386 AD (Clark & Stephenson 1977). Furthermore, this discrepancy suggests the pulsar's current spin period is very near its initial value and that its spin-down energy, $\dot{E} = 6.4 \times 10^{36}$ ergs/s, has remained nearly constant since the supernova explosion.

G11.2−0.3 is an ideal SNR for detailed study due to the observability of emission from all of its components, either at hard X-ray, thermal X-ray or radio frequencies; for a description of its radio and X-ray properties see Tam, Roberts, & Kaspi (2002) and Roberts et al. (2003). The purpose of performing an expansion measurement is to set unambiguous upper and lower limits on its age by examining the expected behaviour of the outer shock during the free expansion (high velocity) and Sedov (low velocity) phases.

2. OBSERVATIONS

We obtained 20- and 6-cm data of G11.2−0.3 taken during 1984−85 (epoch 1) from the VLA archival database. Details of these observations can be found in Table 1 of Tam, Roberts, & Kaspi (2002); data from 1985 February were omitted from this analysis due to poor calibration. Our recent observations made during 2001−02 (epoch 2) at 20 and 6 cm (1465 and 4860 MHz, respectively) are outlined in Table 1.

The data processing was performed using standard procedures within the MIRIAD package (Sault & Killeen 1999), in mosaic and multi-frequency synthesis mode. We performed calibration and editing on each data set individually, before combining all the data of a particular frequency band and epoch. The primary gains were determined using 3C 286 and 3C 48, and phase calibrations were made from observations of 1743−038, 1751−096, 1751−253 and 1820−254 (J2000). Imaging was performed with Robust weighting (Sault & Killeen 1999) as a compromise between maximized signal-to-noise and resolution. We utilized the maximum entropy method (MEM) algorithm for deconvolution (Cornwell, Braun, & Briggs 1999), and applied self-calibration iteratively to improve phase and amplitude calibrations.

[1] Department of Physics and Center for Space Research, Massachusetts Institute of Technology, Cambridge, MA 02139

3. ANALYSIS

The VLA and other radio interferometers have been used to measure the expansion of many SNR such as G11.2−0.3. For a summary of remnants and the techniques used to study them, see Reynoso et al. (1997) and the references therein. Because it is not always possible to make new observations with the same $u-v$ coverage as the archival data, it is important to match up as many of the properties which might affect the quality of our results as best possible, before attempting to directly compare the final images from each epoch. We used the final self-calibrated epoch 2 clean map, after correcting it for primary beam attenuation, as the model for self-calibrating epoch 1 data, as described by Masson (1986) in his cross-calibration method. The purpose of this step was to apply the same residual calibration errors to epoch 1 as existed in epoch 2, thereby minimizing the effects of self-calibration errors on the final subtracted map. In order to match the spatial scales of our images at both epochs, we used MIRIAD modelling procedures to spacially filter the $u-v$ coverage of epoch 2 data to match that at epoch 1, thus creating an epoch 2 dataset with degraded visibility coverage (Gaensler et al. 1999).

Rather than subtract our maps in the $u-v$ plane as done by Masson (1986), we instead mimicked the direct approaches of Moffett, Goss, & Reynolds (1993) and Reynoso et al. (1997) (used to measure the remnant expansions of SN 1006 AD and Tycho's SN (3C 10), respectively) who adopted procedures outlined by Strom, Goss, & Shaver (1982), Tan & Gull (1985) and Dickel et al. (1988). Using the MIRIAD task IMDIFF, we fit the five parameters, described by the maximum likelihood algorithm of Tan & Gull (1985), between our final images: expansion, amplitude (the mean brightness ratio between epochs), x-shift (in the negative right ascension direction), y-shift (declination), and DC offset (the difference in background brightness levels). The best-fit geometrical center of the shell was found to be $< 0\farcs5$ from the position of PSR J1811−1925. We then fixed the amplitude, x-shift, y-shift and offset at the fitted values, performed a series of image subtractions of epoch 1 from epoch 2, each time artificially scaling the epoch 1 image by an expansion factor between 0% and 1.5% in steps of 0.1%, and examined the radial profiles of each difference image for the best-fit expansion factor, or more specifically, the profile that most resembled a line of zero slope. It was evident when examining the difference images that 1.5% was a sufficiently large upper bound on the expansion factor. The difference images were convolved with Gaussians whose FWHM were the same as the synthesized beams' ($19\farcs3 \times 15\farcs3$ at 20 cm, $8\farcs3 \times 7\farcs7$ at 6 cm). Figure 1 shows a map of epoch 2 minus epoch 1 at 20 cm with zero expansion.

We divided the remnant into 24 wedge-shaped regions of 15° azimuthally, and found the average flux of each difference image in annular ring sections as a function of radius between $1'$ and $3'$, recalling that the radius of G11.2−0.3 is $\sim 2\farcm25$ (Tam, Roberts, & Kaspi 2002). The purpose of averaging over wedges, as opposed to simply taking radial cuts, was to smooth out small fluctuations that might have corrupted our data (Strom, Goss, & Shaver 1982). The next task was to determine which of these profiles of average residual flux vs. radius most resembled a flat line. A straightforward χ^2 analysis was not possible, due to our lacking measured uncertainties σ on the residual profile data points. Therefore, we chose to take a modified approach to χ^2-fitting in the hopes of obtaining somewhat legitimate error bars. We weighted each profile data point according to the total intensity in that region at that radius, in lieu of σ, and calculated χ^2 at each expansion value using a flat line as the expected difference profile. To find the best expansion and uncertainties for a particular region, we divided the χ^2 values by the minimum χ^2 of that region; therefore, when we fitted the values to a parabola, its minimum was forced to be near 1. The best expansion was determined by the location of the minima, and the 1σ errors from the location of $\chi^2 = 2$. It should be noted that although these error bars do not represent 1σ in the traditional sense, they do provide a rough indication of each measurement's precision.

4. RESULTS

Figure 2 contains a plot of the best expansion rate estimates as a function of azimuthal angle. As expected, the largest uncertainies correspond to the regions of the shell that are most diffuse, specifically the south-western quadrant (between 90° and 180° W of N). We calculate the weighted mean expansion rate for the entire shell, and find the overall expansion during the ~ 17 yr period separating the epochs to be $(0.71 \pm 0.15)\%$ from 20-cm data and $(0.50 \pm 0.17)\%$ from 6-cm data. This corresponds to a rate of $0\farcs057 \pm 0\farcs012$/yr and $0\farcs040 \pm 0\farcs013$/yr (from 20- and 6-cm data, respectively). The uncertainties represent the RMS deviation about the weighted mean. The expansion parameter $m \simeq (\Delta R/R)/(\Delta t/t)$ will later be used to constrain a rough estimate of the age of G11.2−0.3; here, we assume that the age is equivalent to the time since SN 386 AD, $t = 1616$ yr, and calculate $m = 0.68 \pm 0.14$ (20 cm) and 0.48 ± 0.16 (6 cm). We do not know why there exists a general trend in the difference between the two sets of results, making the expansion at 20 cm appear consistently greater than that at 6 cm; however, we note that the 6-cm data is more susceptible to errors in primary beam correction and incomplete $u-v$ coverage. Even so, the error bars on our data points overlap significantly and the calculated mean expansion values agree within our scatter-based uncertainties.

As an independent check, we compare our measured expansion with the general overall expansion for the entire remnant as fit by IMDIFF. Our results agree with the fit values of 0.7% and 0.5% at 20- and 6-cm, respectively.

5. DISCUSSION

In the first phase of SN evolution, the outer shock wave freely expands into the surrounding medium such that $R \propto t$, and the mass of the ejected material M_{ej} is much greater than the mass of swept up material M_{sw}. As the forward shock begins to decelerate, a reverse shock is driven towards the center of the SNR where it interacts with the PWN, if present (Reynolds & Chevalier 1984; Blondin, Chevalier, & Frierson 2001; van der Swaluw et al. 2001). Eventually these interactions dissipate as the SNR enters the Sedov phase. At this stage, $M_{ej} << M_{sw}$, and the expansion is described by the Sedov solution $R \propto t^{0.4}$ (Sedov 1993). Interactions between the SN shock front and

its ambient medium, which has a density profile thought to be affected by a circumstellar wind produced by pre-supernova mass loss of Type II SN, are currently the subject of extensive investigations (Chevalier 1982; Chevalier & Fransson 1994; Truelove & McKee 1999). The m values predicted for such an environment tend to lie between the extreme values of free expansion and the classical Sedov solution for a constant density medium. Therefore, we will consider these classical definitions for now.

Assuming that G11.2−0.3 has been in either the free expansion or Sedov state continuously since birth, we use our above results and the definition of m to calculate upper and lower constraints on its age, where $\Delta R/R = \Delta\theta/\theta = (0.0071 \pm 0.0015)$ and (0.0050 ± 0.0017). From our 20-cm result, we find upper and lower age limits, corresponding to $m = 1$ and $m = 0.4$ respectively: $t_\uparrow = 2400 \pm 500$ yr, $t_\downarrow = 960 \pm 200$ yr. Likewise, from the 6-cm result we find $t_\uparrow = 3400 \pm 1100$ yr and $t_\downarrow = 1400 \pm 500$ yr. It is immediately obvious that the result of this calculation is highly inconsistent with the characteristic age of PSR J1811−1925, $\tau = 24000$ yr; it is, however, of the same order of magnitude as the time passed since SN 386 AD, and indeed 1616 yr falls easily within these constraints. To eliminate any doubt as to the association between the pulsar and SNR, see the detailed discussion by Kaspi et al. (2001); also discussed are the implications of this age discrepancy on young pulsar astronomy.

Although the PWN is not bright enough to measure a rate of expansion in a similar fashion, we find the presence of flux outlining the general region of the PWN in the zero expansion difference image noteworthy (see Figure 1). The positive emission is indicative of positive expansion; therefore, we conclude that the reverse shock is not compressing the PWN shock front and the SNR is not yet in the Sedov phase. We look to the study of nonradiative SNR evolution by Truelove & McKee (1999), who predict analytically and numerically the expected forward blastwave and reverse shock positions throughout a remnant's lifetime, for a corrobrative explanation. Based on the fact that G11.2−0.3 is likely 1616 yr old, and the expansion parameters we find corresponding to that age, we estimate roughly that the SNR reverse shock radius is currently between 0.5 and 0.8 times the forward blastwave shock radius, assuming a typical ejecta mass for Type II SN of 3−5 $M_\odot$. The ratio of PWN to SNR diameter is ~ 0.28, so the reverse shock would not be expected to have reached the PWN yet. This agrees with what we observe in Figure 1, as well as conclusions outlined in Tam, Roberts, & Kaspi (2002) based on the hydrodynamical simulations of van der Swaluw et al. (2001). Furthermore, we refer to Chevalier (1982), who predicts that the initial expansion phase of a SNR with a red supergiant progenitor can be described by a self-similar solution with a value of $m = 0.9$, as long as both the circumstellar material and the stellar envelope density distributions are power-laws in radius. This is considerably higher than our m estimates, based on $t = 1616$ yr, of roughly 0.48 to 0.68, which suggests that the transition from the initial phase to the Sedov phase is well under way.

5.1. *Distance Estimate*

The distance to G11.2−0.3 is estimated by considering its expansion and angular size. Given the relations $v = mR/t$ and $R = \theta d$, where v is the shell's spatial velocity, θ is the angular radius, and d is the distance to the remnant, it can be seen that

$$d = v\left(\frac{\Delta t}{\theta \cdot \Delta R/R}\right).$$

To find the velocity of the shell, we consider the Mach number of the SNR shock front $M = v/c_s$, where $c_s = \sqrt{\gamma p/\rho}$ is the sound velocity (Longair 1994). Here, $\gamma = 5/3$, and the ratio of pressure to particle mass density is given by $p/\rho = kT_1/\mu m_p$, where T_1 is the temperature of the surrounding material and μm_p is the mean mass per particle ($\mu = 0.6$ for cosmic abundances, m_p is proton mass) (Reynolds et al. 1994). Longair (1997) quotes $T_2/T_1 = 5M^2/16$ for a strong shock in an ideal gas. We measure the temperature behind the shock $T_X \simeq 7 \times 10^6$ K from X-ray spectral fits (Roberts et al. 2003); however, T_2 is the ion temperature and if the electrons are not in full thermal equilibrium with the ions, the observed spectrum may underestimate the shock temperature, and our distance estimate will be too small by a factor of $\sqrt{T_2/T_X}$ (Borkowski, Lyerly, & Reynolds 2001). Combining the above information we find

$$\frac{T_2}{T_1} = \frac{5}{16}\left(\frac{v^2}{5kT_1/3\mu m_p}\right)$$

which gives a lower bound on the distance estimate:

$$d = \left(\frac{16kT_2}{3\mu m_p}\right)^{1/2}\left(\frac{\Delta t}{\theta \cdot \Delta R/R}\right) \gtrsim 3\sqrt{\frac{T_2}{T_X}}\left(\frac{0.0071}{\Delta R/R}\right) \text{kpc}.$$

Green et al. (1988) previously estimated a minimum distance of ~ 5 kpc to the remnant based on its H I spectrum. Fits to the X-ray spectrum with the NPSHOCK model of Borkowski, Lyerly, & Reynolds (2001) suggest that the electrons are near equilibrium; therefore, the distance derived assuming total equilibrium should be very close to that at near equilibrium, and, hence, not much greater than the minimum H I distance.

6. CONCLUSIONS

Based on radio interferometric images of SNR G11.2−0.3 we have made a simple measurement of the outer shell expansion and found a mean rate of $0\farcs057 \pm 0\farcs012$/yr from 20-cm data, and $0\farcs040 \pm 0\farcs013$/yr from 6-cm data. If we compare the expected age of G11.2−0.3, determined by our measurements, with the characteristic age of its associated pulsar PSR J1811−1925, we find an order of magnitude discrepancy; our result further strengthens the growing body of evidence linking G11.2−0.3 with the historical SN of 386 AD. The evolutionary status of this SNR appears to be pre-Sedov, a conclusion that agrees with other observational evidence, as well as theoretical arguments. We also estimate the distance to the remnant based on its X-ray shock velocity to be $\gtrsim 3$ kpc and find it consistent with previously published results.

We wish to thank S. M. Ransom, F. P. Gavriil, V. M. Kaspi, M. Lyutikov and S. P. Reynolds for their helpful comments and suggestions. The National Radio Astronomy Observatory is a facility of the National Science Foundation operated under cooperative agreement by Associated Universities, Inc.

REFERENCES

Blondin, J. M., Chevalier, R. A., & Frierson, D. M. 2001, ApJ, 563, 806
Borkowski, K. J., Lyerly, W. J., & Reynolds, S. P. 2001, ApJ, 548, 820
Chevalier, R. A. 1982, ApJ, 258, 790
Chevalier, R. A. 1984, ApJ, 280, 797
Chevalier, R. A. & Fransson, C. 1994, ApJ, 420, 268
Clark, D. H. & Stephenson, F. R. 1977, The Historical Supernovae (Oxford: Pergamon Press)
Cornwell, T., Braun, R., & Briggs, D. S. 1999, in ASP Conf. Ser. 180, Synthesis Imaging in Radio Astronomy II, ed. G. B. Taylor, C. L. Carilli, & R. A. Perley (San Francisco: ASP), 151
Dickel, J. R., Sault, R., Arendt, R. G., Korista, K. T., & Matsui, Y. 1988, ApJ, 330, 254
Gaensler, B. M., Brazier, K. T. S., Manchester, R. N., Johnston, S., & Green, A. J. 1999, MNRAS, 305, 724
Green, D. A., Gull, S. F., Tan, S. M., & Simon, A. J. B. 1988, MNRAS, 231, 735
Kaspi, V. M., Roberts, M. E., Vasisht, G., Gotthelf, E. V., Pivovaroff, M., & Kawai, N. 2001, ApJ, 560, 371
Kothes, R. & Reich, W. 2001, A&A, 372, 627
Longair, M. S. 1997, High Energy Astrophysics, Vol. 1 (2nd ed.; Cambridge: Cambridge University Press)
Longair, M. S. 1994, High Energy Astrophysics, Vol. 2 (2nd ed.; Cambridge: Cambridge University Press)
Masson, C. R. 1986, ApJ, 302, L27
Moffett, D. A., Goss, W. M., & Reynolds, S. P. 1993, AJ, 106, 1566
Reynolds, S. P. & Chevalier, R. A. 1984, ApJ, 278, 630
Reynolds, S. P., Lyutikov, M., Blandford, R. D., & Seward, F. D. 1994, MNRAS, 271, L1
Reynoso, E. M., Moffett, D. A., Goss, W. M., Dubner, G. M., Dickel, J. R., Reynolds, S. P., & Giacani, E. B. 1997, ApJ, 491, 816
Roberts, M. S. E., Tam, C. R., Kaspi, V. M., Lyutikov, M., Vasisht, G., Pivovaroff, M., Gotthelf, E. V., & Kawai, N. 2003, ApJ, 588, 992
Sault, R. J. & Killeen, N. E. B. 1999, The MIRIAD User's Guide. Australia Telescope National Facility, Sydney (http://www.atnf.csiro.au/computing/software/miriad)
Sedov, L. I. 1993, Similarity and Dimensional Methods in Mechanics (10th ed.; Boca Raton, FL: CRC Press, Inc.)
Strom, R. G., Goss, W. M., & Shaver, P. A. 1982, MNRAS, 200, 473
Tam, C., Roberts, M. S. E., & Kaspi, V. M. 2002, ApJ, 572, 202
Tan, S. M. & Gull, S. F. 1985, MNRAS, 216, 949
Torii, K., Tsunemi, H., Dotani, T., & Mitsuda, K. 1997, ApJ, 489, L145
Torii, K., Tsunemi, H., Dotani, T., Mitsuda, K., Kawai, N., Kinugasa, K., Saito, Y., & Shibata, S. 1999, ApJ, 523, L69
Truelove, J. K. & McKee, C. F. 1999, ApJS, 120, 299
van der Swaluw, E., Achterberg, A., Gallant, Y. A. & Tóth, G. 2000, A&A, 380, 309
Vasisht, G., Aoki, T., Dotani, T., Kulkarni, S. R., & Nagase, F. 1996, ApJ, 456, L59

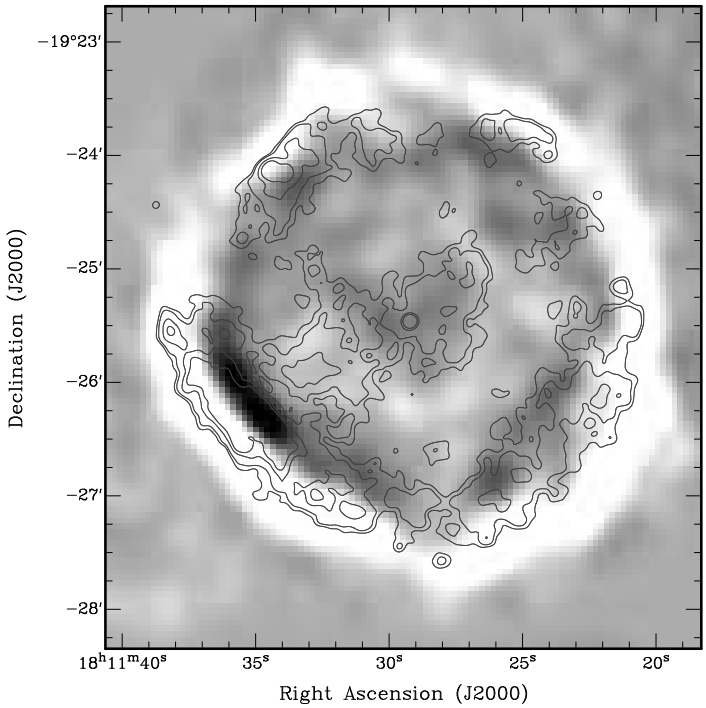

FIG. 1.— 20-cm difference map of epoch 1 image subtracted from epoch 2 image, with no expansion applied. Positive (white) emission on the outer shell and negative (black) emission on the inner shell indicate that a noticeable amount of expansion has occured between epochs. Contours of the Chandra 0.6−1.65 keV X-ray image, smoothed with a 5″ Gaussian, are shown at levels of 1.5, 2, 3.5, and 5×10^{-6} photons/cm^2/s/pixel. The extended structure in the interior of the X-ray shell is thought to be the PWN forward shock; this is discussed in Roberts et al. (2003).

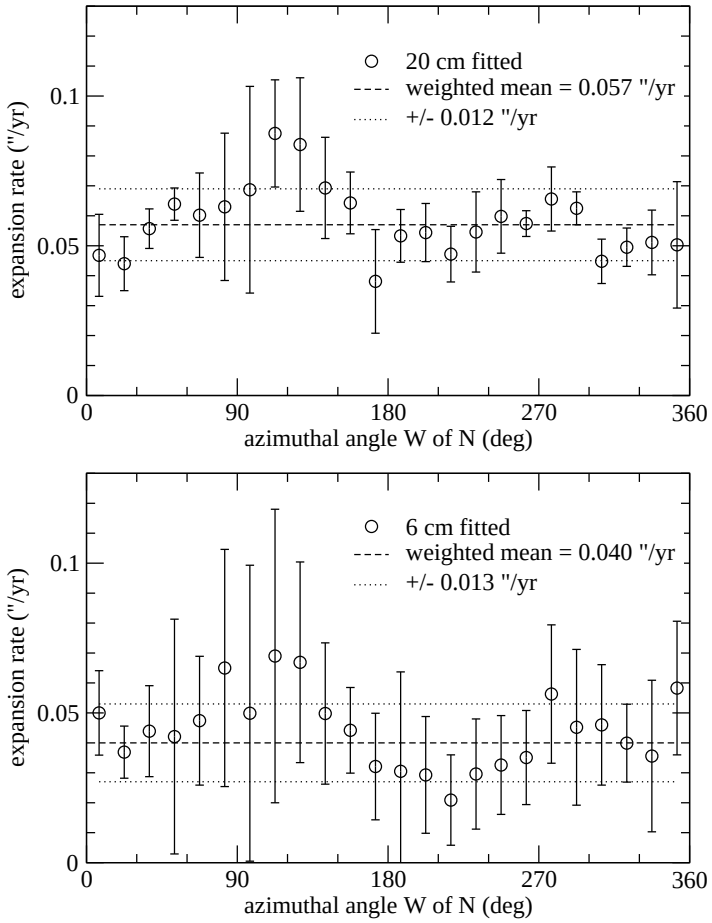

FIG. 2.— Azimuthal variation of average expansion rate, from 20- (top) and 6-cm (bottom) data. The fitted values (circles) determined by a pseudo χ^2 analysis with $\sim 1\sigma$ error bars are shown (solid lines), as is the weighted mean (dashed line) and its RMS scatter (dotted lines) for comparison.

TABLE 1
VLA OBSERVING PARAMETERS FOR EPOCH 2

Observing Date	Array Config.	Frequencies (MHz)	Bandwidth (MHz)	Time on Source (min)
2001 Jun 26	CnB	1465	25	63
2001 Jun 26	CnB	4835, 4885	25	81
2001 Aug 03	C	1465	25	60
2001 Aug 03	C	4835, 4885	25	66
2001 Sep 24	DnC	1465	25	92
2001 Sep 24	DnC	4835, 4885	25	99
2002 May 24	BnA	1465	25	98
2002 May 24	BnA	4835, 4885	25	118